Novel Orthogonal Random Phase-Coded Pulsed Radar for Automotive Application

Xu Zhihuo*① Shi Quan① Sun Ling②

①(*School of Transportation, Nantong University, Nantong* 226019, *China*)

②(*Jiangsu Key Laboratory of ASIC Design, Nantong* 226019, *China*)

Abstract: In contrast to remote sensing radar, automotive radar focuses on the detection of short-range targets in the 0–1000 m range. Conventional automotive pulsed radar usually uses a monostatic antenna and it requires high peak power for the transmission of the short duration pulses to reliably detect targets at close range with a high resolution. Unfortunately, it is difficult and expensive to generate high-powered pulses on the nanosecond scale. Meanwhile, the existing automotive radars suffer from bottlenecks, *i.e.*, spatial resolution, sidelobe levels, and Inter-Sensor Interference (ISI). To overcome the above challenges, a bistatic antenna to transmit and receive large time-bandwidth product waveforms is firstly proposed in this paper. Secondly, high spatial resolution is implemented using a Digital Beam Forming (DBF) transmitter and the high range resolution is achieved by using the pulse compression technique. Additionally, the radial velocity of the target is calculated by applying pulse Doppler processing. Finally, to deal with the sidelobe effect of impulse response function of point target and the interference arising from neighboring radars, novel Orthogonal Random Phase-Coded (ORPC) radar signals are presented. Using these ORPC signals, the impulse response function of the radar can achieve a peak sidelobe ratio of –45 dB without any loss in the signal-to-noise ratio. Most importantly, interference can be significantly reduced by using the proposed signals. Extensive simulations demonstrate the effectiveness and advantages of the proposed radar.

Key words: Digital Beam Forming (DBF); Inter-Sensor Interference (ISI) reduction; Sidelobe mitigation; Orthogonal Random Phase-Coded (ORPC); Automotive pulsed radar

DOI: 10.12000/JR17083

Reference format: Xu Zhihuo, Shi Quan, and Sun Ling. Novel orthogonal random phase-coded pulsed radar for automotive application[J]. *Journal of Radars*, 2018, 7(3): 364–375. DOI: 10.12000/JR17083.

引用格式：许致火, 施佺, 孙玲. 一种正交随机相位编码的新型汽车脉冲雷达[J]. 雷达学报, 2018, 7(3): 364–375. DOI: 10.12000/JR17083.

一种正交随机相位编码的新型汽车脉冲雷达

许致火① 施 佺① 孙 玲②

①(南通大学交通学院 南通 226019)

②(江苏省专用集成电路设计重点实验室 南通 226019)

摘 要：相比遥感雷达，汽车雷达探测距离为0–1000 m近距离的车辆及行人等目标。常规的单天线汽车脉冲雷达通常发射纳秒级的短脉冲以实现近距目标的高分辨率探测。但在工程上实现纳秒级的高功率发射信号是非常困难的并需要很高的成本。另外，现有的汽车雷达存在空间角度分辨率低、点目标脉冲响应函数旁瓣高及汽车雷达间

Manuscript received September 12, 2017; Revised April 03, 2018; Published online June 05, 2018.

*Communication author: Xu Zhihuo.

E-mail: xuzhihuo@gmail.com.

Foundation Items: The National Natural Science Foundation of China (61771265), The Open Fund of the Nantong University-Nantong Joint Research Center for Intelligent Information Technology (KFKT2016A11), The Nantong Natural Science and Technology Project (GY12016017), The Natural Science Fund for Colleges and Universities in Jiangsu Province (17KJB510047), The Scientific Research Start-up Foundation for Talent Introduction of Nantong University (17R30).

相互强干扰的瓶颈问题。为克服这些难题，论文首先提出双天线脉冲雷达技术，使得雷达在测量发射大时宽脉冲信号成为可能。其次，通过数字波束形成技术实现高的空间分辨率，运用脉冲压缩技术实现距离向高分辨率，采用脉冲多普勒技术计算得到高分辨率的径向速度场。最后，为克服点目标脉冲响应函数旁瓣效应及汽车雷达间相互干扰的问题，提出了一种新的随机相位编码雷达信号。采用提出的雷达信号，汽车雷达间的强干扰可被有效抑制，并且在不损失信噪比的情况下，雷达的点目标脉冲响应函数的峰值旁瓣比可达–45 dB。大量的数值仿真实验验证了提出方法的有效性及先进性。

关键词：数字波束形成；雷达间干扰抑制；旁瓣抑制；正交相位编码；汽车脉冲雷达

中图分类号：TN951 **文献标识码**：A **文章编号**：2095-283X(2018)03-0364-12

1 Introduction

Advanced Driver Assistance Systems (ADASs) have significantly improved the safety of driver and surrounding traffic in the past two decades[1–5]. These systems focus on lane departure warning, blind-spot detection, Automatic Cruise Control (ACC), road condition and traffic light recognition, just to name a few. The pinnacle of ADASs is fully autonomous driving. Basically, the success of ADASs and self-driving vehicle systems depends on precise and robust localization of other vehicles, pedestrians and the surrounding environment of a host vehicle. To this end, many on-board sensors such as camera, Light Detection And Ranging (LiDAR), infrared, ultrasonic sensor, and wireless sensors have been developed to detect other vehicles or pedestrians[1–9]. Furthermore, to increase the robustness of ADASs, multi sensors are used to provide reliable information[8–11]. Compared with other types of sensors for automotive applications, the microwave radar sensor has its own uniqueness in sensing capability independent of daylight and weather conditions. Consequently, it is undoubtedly an integral part of any multipurpose sensor fusion system, could be used to achieve a fully autonomous driving vehicle[1–11].

From the perspective of modulation schemes, the automotive radar can be categorized into three types: (1) Linear Frequency Modulated Continuous Wave (LFMCW); (2) Frequency Shift Keying (FSK); and (3) pulsed Doppler[1–4]. For reason of economy, the LFMCW radar has been the most widely used in automotive applications. These sensors are very simple to implement, providing direct measurement of the radial velocity and the range of target in a high accuracy. Despite its obvious merits, when several targets are in the radar beam, the velocity measurement fails. Furthermore, these radars have no azimuth angular measurements of the detected targets, resulting in a very limited spatial resolution. In addition, their performance can be strongly degraded because of the interfering signals that are produced by neighboring radars operated at the same frequency band. The FSK radar is implemented by using a multi-frequency Continuous Wave (CW) transmissions. Pulsed Doppler radars have also long been employed for automotive applications. They transmit pulse of short duration. Its high peak power must be required to reliably detect the targets at long distance. However, it is difficult and expensive to generate high-powered pulses on the order of nanoseconds.

The microwave radar detection can provide real time road scenario information ahead of a vehicle in any weather conditions even in which electro-optical sensors fail. Many contributions have been made to the development of automotive radar. However, many fundamental issues for the radar sensor still remain largely open. These include multipath reflection, field of view, azimuth resolution enhancement, aspects of Inter-Sensor Interference (ISI), waveform design, system sidelobe levels of Impulse Response Function (IRF), and radar system architectures, to name a few.

A road surface can cause multipath reflection, degrade the received power, and reduce the detection probability. The authors in Ref. [12] develop a one-transmitter-two-receiver 24-GHz FMCW radar architecture with spatial diversity to reduce the multipath reflection.

It is well known that radar must detect not only the range and radial velocities but also azimuth of targets. To obtain a large field of view in front of the vehicle, a conformal array design is applied[13].

By applying a high-resolution spectral estimator called APES, high resolution with low sidelobe levels for both range and azimuth can be obtained for a FSK radar. However, this is not enough to discriminate the lane where the vehicles or pedestrians are moving on. These reasons have led to the concept of Beam Forming (BF) technique. Switch-antenna array FMCW radar system is composed to perform accurate and agile beam scanning and target direction determination[14,15].

Our approach to high spatial resolution is based on the electronically scanning the beam of the antenna. Several recent efforts are utilizing Digital Beam Forming (DBF)[16,17]. Despite these sensors electronically scan in azimuth, the azimuth resolution is also not adequate to reliably discriminate the targets.

The radars are typically installed on a vehicle. When nearby radar operate in the same frequency band with the host radar, the inter-sensor interference appears. To deal with interfering signals produced by neighboring radars, radars employing coded signal like chaotic signals and Pseudo-Noise (PN) sequence in Direct-Sequence (DS) configuration have been proposed[18]. The coded signals are the radar "signature", exhibiting good correlation properties. This characteristic of the signal allows sensor to measure the range and velocity of a vehicle by selecting its echo among interfering signals. The authors in Ref. [19] adopt distributed Time Division Multiple Access (TDMA) method to handle with ISI in the ultrasonic sensors. Moreover, the effect of ISI malfunction on the radar has been covered in Ref. [20] by using an auxiliary receiver.

Furthermore, it is essential to develop a high resolution with low sidelobe levels. A system IRF with low sidelobes is of great importance in radar images because high sidelobes will interfere with nearby scatterers. The low sidelobe is a key issue of detecting the targets with low reflectivity like pedestrians, in order to suppress the sidelobe of the nearby targets with high reflectivity such as vehicles, and metal guardrails of roads, see Fig. 1. For the LFMCW radar, the Peak SideLobe Ratio (PSLR) level of the beat signal of point scatterers in the spectral domain is typical –13.25 dB. Similarly,

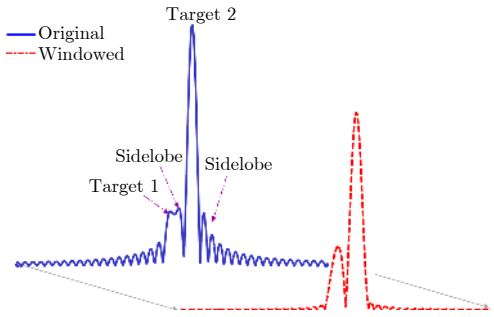

Fig. 1 Conceptual sketch of reducing the effect of sidelobes

the pulsed Doppler radar also suffer the same effect of the sidelobes. To reduce the sidelobes, a symmetrical window processing is commonly applied in the spectra domain of the radar data. In general, the lower level of sidelobes are achieved at the cost of broadening of main-lobe width of IRF that governs the range resolution of the underlying sensors.

Moreover, the window processing degrades the Signal to Noise Ratio (SNR) of the radar system. To analyze the loss of SNR in details, we reviewed the theory of the matched filter firstly. If one echo signal $s_r(t)$ plus additive white Gaussian noise with two-sided Power Spectral Density (PSD) $\frac{N_0}{2}$ goes through a filter with an IRF of $h(t)$, then the variance of the output noise is $\sigma^2 = \frac{N_0}{2}\int_{-\infty}^{\infty}|h(t)|^2\mathrm{d}t$. The output signal is denoted as $y(t)$. According to the Cauchy-Schwarz inequality, to maximize the SNR $y(t_0)/\sigma$ at time t_0, choice of the filter follows $h(t) = s_r(t_0 - t)$. Hence, the filter $h(t)$ that is matched to $s_r(t)$ at time t_0, called matched filter.

Regarding the window processing, the filter can be formulated as $h(t) = w(t)\, s_r(t_0 - t) \neq s_r(t_0 - t)$, where $w(t)$ is a symmetrical window. It is obviously that the filter $h(t)$ is mismatched to $s_r(t)$. Consequently, the output SNR value is not a maximum. The decrease of SNR can be quantified as $\mathrm{SNR}_D = 10\lg\dfrac{\left|\int_0^T w(t)\mathrm{d}t\right|^2}{T\int_0^T w(t)^2\mathrm{d}t}$, where T is the length of the window[21](Richards 2005, Section 5.3.1).

As shown in the Fig. 2, this process leads to

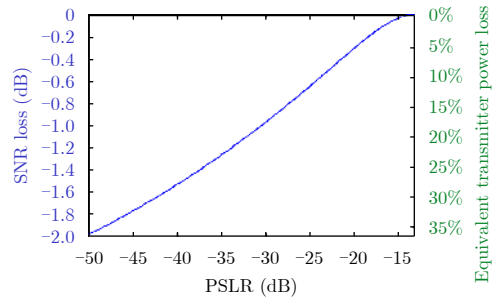

Fig. 2 SNR loss and equivalent transmitter power loss versus PSLR in the window processing

a typical 1–2 dB of SNR loss, which is equivalent to a range of 20%–37% decrease in transmitter power. Consequently, the probability of false alarm of the sensor is increased.

In this paper, we propose a new architecture for pulsed Doppler imaging radar sensor and a new modulation scheme for the transmitted signals. Nevertheless, several challenges arise for pulse Doppler radar design for automotive applications. First, because the automotive radar focuses on detection of the targets at close range, we propose bistatic antenna architecture, one is for the transmitter, and the other is used for the receiver, operating at the same time. This is a difference with present pulsed radar in automotive applications. Using bistatic antenna allows sensor transmit large time-bandwidth product signals. Hence, the range of targets is measured by using Pulse Compression (PC) method. It offers clear benefits of high resolution detection of close range targets. On the other hand, to achieve high resolution in azimuth, we adopt DBF technique to electronically steer the beam of a highly directive transmitter antenna, significantly improving the azimuth resolution. The radial velocity of the targets are estimated via pulse Doppler processing.

Another contribution of our work is designing of Orthogonal Random Phase-Coded (ORPC) signals. The proposed signal offers the radar system a very low sidelobe level without any loss of SNR. Most importantly, based on the proposed ORPC signals, interference mitigation schedule is presented.

Despite many contributions have been done in the field of the automotive radar sensor, to our best knowledge, there has been no work that takes the bottlenecks of spatial resolution, sidelobe level of IRF and ISI issues as a whole into consideration. Compared with the current state of the arts, the proposed radar sensor: (1) satisfies the requirement of simultaneously imaging the target range together with speed in high resolution; (2) exhibits the characteristics of simultaneously reducing the sidelobe level and persevering the SNR for the system; and (3) reduces the interference from neighboring radar sensor significantly.

The remainder of this paper is organized as follows. Section 2 presents the proposed methodology, including the new radar sensor system and signal processing, the ORPC signals and the interference-free schedule. Section 3 demonstrates the numerical results of the high resolution radar images with lower sidelobe levels without any loss of SNR, discriminating the pedestrian from the vehicles clearly. Next, the results on ISI mitigation are reported in this section. Conclusion is drawn in Section 4.

2 The Proposed Radar System and Signal Processing

2.1 Architecture of proposed radar

Fig. 3 shows a schematic of the proposed imaging radar for measuring target range, azimuth, and speed. A DBF antenna with a narrow beam width is used as electronical scanning transmitter to improve the azimuth resolution. A DBF transmitter can be formulated as a spatial filter that operates on the outputs of a sensor array in order to form a desired directivity pattern. We adopt an omni-directional linear antenna array of N transmitting antenna elements sharing one single receiving antenna. For reason of cost and complexity, the receiving antenna is designed to be omni-directional, allowing the receiver to listen echoes from different azimuth. The transmitting antenna elements are uniformly spaced d apart. According to the geometry in Fig. 3, the vector $\boldsymbol{w} = \{w_1, w_2, \cdots, w_N\}$ generated by digital phase shifter is calculated as

$$w_n = \mathrm{e}^{-\mathrm{j}(n-1)\kappa d \sin(\theta_{\mathrm{az}})} \tag{1}$$

where the wavenumber $\kappa = 2\pi/\lambda$, θ_{az} is the desired direction of azimuth, and λ is the wavelength of the transmitted signal. Consequently, the Array Factor (AF) is formulated by:

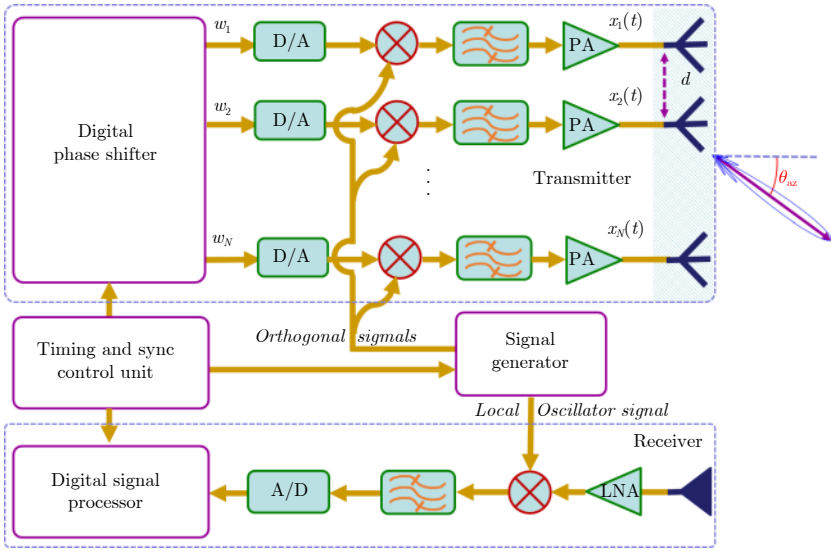

Fig. 3 Schematic of the proposed radar

$$\mathrm{AF}=\left|\sum_{n=1}^{N}\mathrm{e}^{\mathrm{j}\kappa d(n-1)\{\sin(\theta)-\sin(\theta_{\mathrm{az}})\}}\right|=\frac{\sin(0.5N\psi)}{\sin(0.5\psi)} \quad (2)$$

where θ is the angle of azimuth, and $\psi=\kappa d\cdot\{\sin(\theta)-\sin(\theta_{\mathrm{az}})\}$. According to Eq. (2), the maximum radiation can be steered to the desired direction of azimuth θ_{az}, by programming the phase shift vector $\boldsymbol{w}$ for the scanning array.

2.2 Design of ORPC signals

The output signals from signal generator are divided into the following two parts: orthogonal signals to modules of up-conversion for transmission and a local oscillator signal used by receiver to down-convert echoes from the receiving antenna. At each instant time t, the oscillator signal is expressed as

$$s_{\mathrm{osc}}(t)=\exp(\mathrm{j}2\pi f_0 t)=\exp\{\mathrm{j}2\pi t(c/\lambda)\} \quad (3)$$

where f_0 is the carrier frequency and c is the velocity of light.

Most importantly, to simultaneously deal with ISI issues, the orthogonal signal at the current pulse is orthogonal with the next and the previous one. These signals are large time-bandwidth product waveforms using Frequency Modulated (FM) techniques, in order to increase the range resolution as well as the SNR. The i-th signal of M orthogonal signals can be formulated as

$$s_i(t)=\exp\{\mathrm{j}2\pi f_0 t+\phi_i(t)\},\quad 0\le t\le\tau,\quad i=1,2,\cdots,M \quad (4)$$

where τ is the pulse duration, $\phi_i(t)$ is the modulated phase. Because of orthogonality, these signals follow

$$\begin{cases}\int s_i(t)s_i^*(t)\mathrm{d}t=A\\ \int s_i(t)s_k^*(t)\mathrm{d}t=0,(i\ne k)\end{cases},\quad 0\le t\le T,\quad i=1,2,\cdots,M \quad (5)$$

where A is the energy of the i-th signal.

For the ORPC signal, the time-frequency functions can be any forms without analytic expression. This paper designs ORPC signals, using one phase retrieval method referred to as the Gerchberg-Saxton (GS) algorithm[22]. First, we define the PSD $|S(k)|$ of the ORPC, using a symmetrical window. Next, the phases of the signals $s(t)$ with orthogonality are explored as follows:

(1) Choose initial $s_i(n)=\exp\{\mathrm{j}\phi(n)\}, i=0$, where $\phi(n)$ is a random phase. The convergence threshold is set as ϵ=1e–16.

(2) Fourier Transform (FT) $s_i(n)$ to obtain $X_i(k)$: $X_i(k)$=FT$\{s_i(n)\}$.

(3) Form an estimate of the FT of $s(n)$, using the current Fourier phase of $X_i(k)$, but replacing the magnitude of the resulting computed FT with the desired spectral density: $\hat{S}(k)=|S(k)|\dfrac{X_i(k)}{|X_i(k)|}$.

(4) Inverse Fourier transform (IFT) $\hat{S}(k)$ to obtain the new estimate of ORPC signal: $s_{i+1}(n)=\mathrm{IFT}\{\hat{S}(k)\}$.

(5) Repeat Step (2)–(5) until the error $\sum_k\left||X_i(k)|-|S(k)|\right|^2\le\epsilon$.

Thanks to no uniqueness solutions, the GS algorithm will produce a group signal with different

phases, but sharing the same spectral density. In the next section, we will demonstrate the orthogonality of these ORPC signals. In practice, the above method produces the discrete values of the ORPC signals. Then, the ORPC transmission signals of the radar sensor can be conveniently obtained by using large-scale Field Programmable Gate Arrays (FPGA) circuits and Digital-to-Analog Converters (ADC).

2.3 Timing for mitigating interference

As shown in Fig. 4, the timing and synchronization unit controls the three parts of the sensor system in a collaborative way as follows: (1) guides the digital phase shifter for generating a progressive phase vector $\boldsymbol{w}$; (2) controls the orthogonal signals to be successively emitted one pulse by one pulse; and (3) synchronizes the Digital Processing Processor (DSP) with the transmitted signals, to select the corresponding signal for PC in DSP.

The receiver is always being turned on to listen the echoes from the targets at the close range. The Pulse Repetition Time (PRT) is chosen to be larger than twice the propagation time of the transmitted signal to the maximum detection range of the sensor.

Because of using the omni-directional receiving antenna, besides the echoes of the targets, the interference signal can also be collected to the radar receiver. Consequently, the performance of sensor is strongly degraded. Fortunately, these undesired signals can be reduced significantly by using the proposed signals with orthogonality. Based on the proposed ORPC signals, interference mitigation schedule is presented as follows. We choose M signals generated by the above proposed approach as the sensor transmitted signals. The different ORPC pulses are transmitted during each Pulse Repetition Interval (PRI). In the N adjacent PRIs, we transmit N different ORPC waveforms $s_1(t)$, $s_2(t)$,$\cdots$, $s_M(t)$ which satisfy the condition of the Eq. (5). The ORPC signals are the "signature" of each transmitted pulses, exhibiting good orthogonal properties. Therefore, the inter-sensor interference can be reduced by using the ORPC signals.

2.4 Signal processing

The radar digital signal processor consists of two functions: (1) range imaging; and (2) velocity mapping of the targets. Consider a target located at range R and azimuth θ at time t, moving at speed v. We define the coherent processing interval (CPI) as N PRT. It means that the speed is assumed to be constant throughout N sweeps of the sensor antenna. The delay between the radar and the target at the k-th sweep is defined as

$$\begin{aligned}\tau_{\mathrm{d}}(t+k\mathrm{PRT}) &= 2R(t+k\mathrm{PRT})/c \\ &= \frac{2R_0}{c} - \frac{2v\cos(\theta)(k\mathrm{PRT})}{c}\end{aligned} \tag{6}$$

We define a slow time $\eta = k\mathrm{PRT}$ for the azimuth. After down-convert in the receiver, the echoes corresponding the i-th transmission can be expressed as

$$\begin{aligned}r_i(t,\eta) = \exp\left\{\mathrm{j}\frac{-4\pi R_0}{\lambda}\right\}\exp\left\{\mathrm{j}\frac{-4\pi v\cos(\theta)\eta}{\lambda}\right\} \\ \cdot\exp\left\{\mathrm{j}2\pi\phi_i\left(t-\frac{2R_0}{c}-\frac{2v\cos(\theta)\eta}{c}\right)\right\}, \\ 0\le t\le\tau,\quad i=1,2,\cdots,M\end{aligned} \tag{7}$$

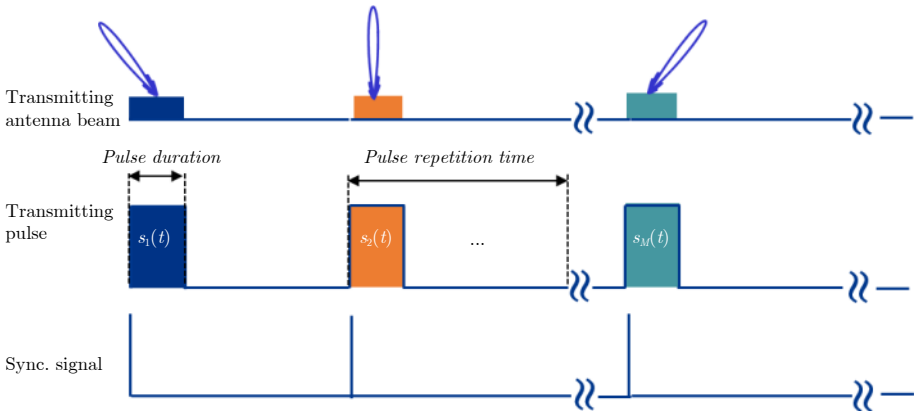

Fig. 4 System timing and synchronization diagram of the proposed radar

Because $v \ll c$, the delay term of $[2v\cos(\theta)\eta]/c$ in the last exponential term can be ignored. Hence, Eq. (8) is approximated as

$$r_i(t,\eta) \simeq \exp\left\{\mathrm{j}\frac{-4\pi R_0}{\lambda}\right\}\exp\left\{\mathrm{j}\frac{-4\pi v\cos(\theta)\eta}{\lambda}\right\} \cdot \exp\left\{\mathrm{j}2\pi\phi_i\left(t-\frac{2R_0}{c}\right)\right\}, \quad 0 \le t \le \tau, \quad i=1,2,\cdots,M \tag{8}$$

As shown in Fig. 5, the range imaging is implemented by using PC technique. A Fast Fourier Transform (FFT) is used to convert echoes into the frequency domain. The output of PC is defined as

$$s_{\mathrm{pc}}(t,\eta) = \mathrm{IFFT}\Big\{\mathrm{FFT}[r_i(t,\eta)]\cdot\mathrm{FFT}^*[s_{\mathrm{ref},i}(t)]\Big\}, \quad 0 \le t \le \tau, \quad i=1,2,\cdots,M \tag{9}$$

where $s_{\mathrm{ref},i}(t)$ is the i-th matched filter, defined as

$$s_{\mathrm{ref},i}(t) = \exp\{\mathrm{j}\phi_i(t)\}, \ 0 \le t \le \tau, \ i=1,2,\cdots,M \tag{10}$$

Then, the first step of pulse Doppler processing is applied to range compressed data in a CPI by using the FFT as

$$s_{\mathrm{pc}}(t,f_\eta) = \mathrm{FFT}(s_{\mathrm{pc}}(t,\eta)) \tag{11}$$

Finally, the velocity of the target is estimated as follows

$$s_v(t,v_r) = -\frac{\lambda}{2\cos(\theta)}\cdot\arg\max_{f_\eta}\Big\{|s_{\mathrm{pc}}(t,f_\eta)|\Big\} \tag{12}$$

3 Simulation Results

The proposed radar and signals are evaluated by simulation in terms of the following four aspects: (1) The orthogonality and ambiguity function of the proposed signals; (2) sidelobe reduction; (3) simultaneously imaging the target range together with speed in high resolution; and (4) mitigation of interference from neighboring radars.

3.1 Results of OPRC signals

To verify the orthogonality of the proposed signals, the numerical experiments have been conducted. The proposed approaches can produce any large time-bandwidth waveforms. Here, the pulse duration and the bandwidth of signal are set as 2.0 μs and 600 MHz, respectively, as an experimental study. By taking the necessary storage and computation of the radar signals into consideration, the oversampling factor is chosen to be 1.2, to obtain efficient use of the signal samples, but to still have a capable gap in the spectrum for sampling. Hence, the sampling rate is chosen as 720 MHz for the signals. Fig. 6 shows the numerical results of the proposed signals.

Because the Linear Frequency Modulated (LFM) signals are common in radar sensor, we compare the proposed ORPC signals with Orthogonal Linear Frequency Modulated (OLFM). The OLFM signals are defined as

$$s_i(t) = \exp\Big\{\mathrm{j}\pi K_i^2 t\Big\}, \ 0 \le t \le \tau, \quad i=1,2 \tag{13}$$

where the chirp-rate $K_1 = K$, and $K_1 = -K$. The above two signals can be easily verified to be orthogonal, following the requirement of Eq. (5). The OLFM signals suffer the same effect of the sidelobes as well as LFM signal. The PSLR is –13.25 dB in the auto correlation of OLFM signals. Generally, the window processing applies weights to the signal spectrum, reducing sidelobe levels. Unfortunately, the window processing led to a loss of SNR.

Interestingly, the ORPC signal exhibits arbitrary waveforms. However, the PSD of these signals are

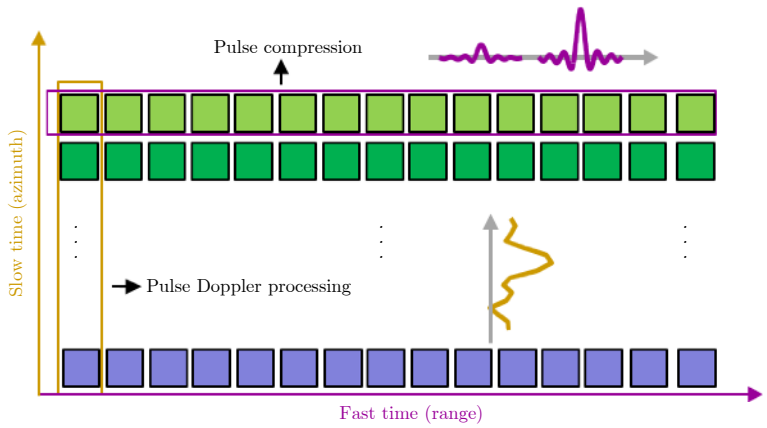

Fig. 5 Conceptual sketch of signal processing for the proposed radar

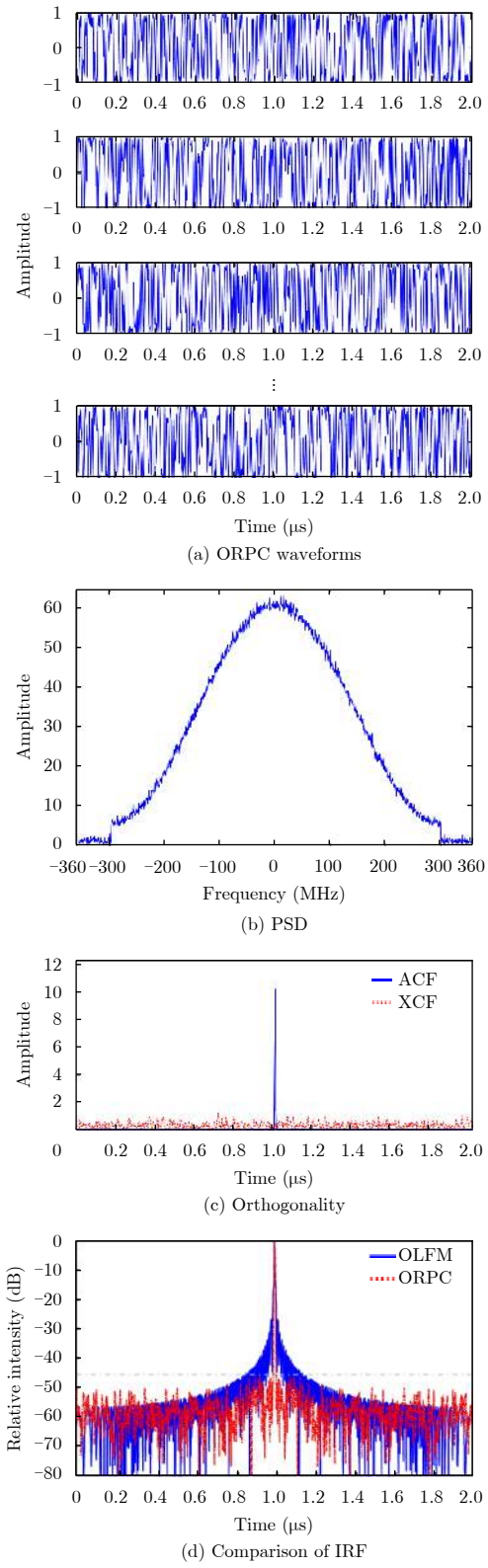

(a) ORPC waveforms

(b) PSD

(c) Orthogonality

(d) Comparison of IRF

Fig. 6 The performance of the proposed waveforms

the same and a typical spectral of the ORPC signal, shown in the Fig. 6(b). Fig. 6(c) demonstrates the orthogonality of the proposed signals. The ACF of ORPC signals is similar to delta function impulse response. On the other hand, the outputs of the across correlation function (XCF) of the proposed signals are nearly zeros, and much small than the peak values of the ACF. Most interestingly, the peak sidelobe levels of IRF of ORPC are much lower than that of the OLFM signals. The PSLR of ORPC is –45 dB, but the broaden factor of the Main lobe Width (MW) of ORPC is 1.5 by referring to the MW of OLFM. The PSLR of the IRF of the OLFM signal can be achieved to –45 dB by applying window weighting. However, this processing leads to a 1.9 dB of SNR loss.

Furthermore, it is essential to use the ambiguity function to analyze the behavior of the proposed signals with their matched filters. For the proposed pulsed radar sensor, the ambiguity function is defined as

$$A(t,F_{\mathrm{d}})=\int_{-\infty}^{\infty}\left(\sum_{i=1}^{M}s_i\left(t-(i-1)\,\mathrm{PRT}\right)\right)\cdot\left(\sum_{k=1}^{M}s_k^{*}\left(s-t-(k-1)\,\mathrm{PRT}\right)\right)\mathrm{e}^{\mathrm{j}2\pi F_d s}\mathrm{d}s \tag{14}$$

where s^* is the conjugate operation. According to Eq. (14), $M=2$ for the OLFM signals. We chose three ORPC signals for caculating array factor, hence $M=3$.

Fig. 7 illustrates the ambiguity function of the proposed ORPC waveforms. The ouputs of Zero-Doppler cut of the ambiguity function for the ORPC waveforms are the same as the ACF shown in Fig. 6(c). Consequntly, these profiles are not plotted again. On the other hand, the Doppler effect of the OLFM signals results in expanding the central portion and prodcuing a sidelobe structue. In contrast to the OLFM signals, the ambiguity function of the ORPC signals generates a nearly ideal like "thumbtack" structure, showing a generally low and relatively uniform sidelobe structure thoughout the delay-Doppler plane.

3.2 Sidelobe reduction

For automotive applications, the reduction of sidelobe is of great importance for detecting the targets with low reflection like pedestrian, in order to suppress the sidelobe effect of nearby targets with high reflection such as vehicles, and metal guardrails of road.

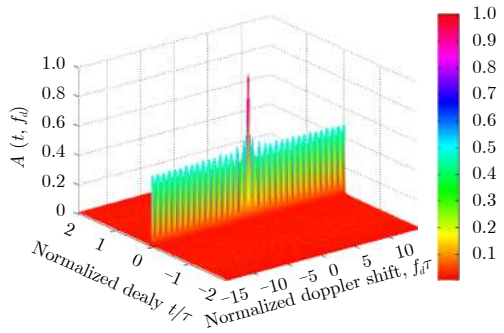

(a) OLFM

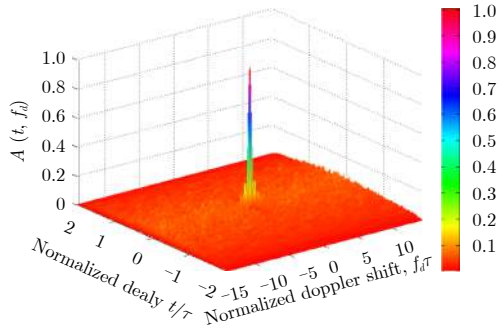

(b) ORPC

Fig. 7 Ambiguity functions

The ORPC waveforms shown in Fig. 6(a) are used as transmitted signals. Hence, the range resolution is 0.25 m. We take 24 GHz carrier wave as an example for the proposed imaging radar. The pulse repeat frequency is 20 kHz. The coherent processing interval is chosen as 16 PRT. The beam-width of transmitted antenna is expected to be 5°. The progressive phase interval is set as 0.125° for the digital phase shifter.

To show the sidelobes clearly, a point target focused by the proposed sensor are analyzed by selecting a 31×31 window centered on the peak, and up sampling by a factor of 16. The results are reported in Fig. 8. The plots obviously suggest that sidelobes levels are reduced effectively in range by using the ORPC signals. The PSLR of the OLFM radar is –13.25 dB. Conversely, the sidelobe of the ORPC radar are significantly reduced. The levels are below –42 dB, agreeing with the theoretical value. Referred to the mainlobe width of OLFM, the broaden factor of the mainlobe width of ORPC is 1.5, resulting in that the range resolution of ORPC is 0.375 m.

3.3 High resolution imaging

A representative experiment is considered. The typical road environment is illustrated in Fig. 9, where a pedestrian, and a car equipped with one interfering radar sensor are present. The car target is located at 26.5 m range, moving in the same direction at 20 m/s (72 km/h). The size of the car is 1.5 m in height and 2.0 m in width. The pedestrian is located at 24.5 m range, running in the opposite direction at 1 m/s. First, let us consider a case without interference signals. Using the proposed imaging radar sensor, the radar images of the targets are processed and shown in Fig. 10. Obviously, the image exhibits high resolution. The pedestrian and car are discriminated clearly. The estimated velocities are mapping the velocity into the radar reflectivity image of targets detected by a canny edge detector. The expected value of the estimated velocity of the car and pedestrian is 20.06 m/s and –0.97 m/s, respectively, at a system SNR of 30 dB. The Mean Square Error (MSE) of the estimated velocity is 0.14 m/s.

3.4 Mitigation of interferences

The inter-sensor interference appears if nearby radar operate in the same frequency band with the host radar. Similarly, thanks to the orthogonality

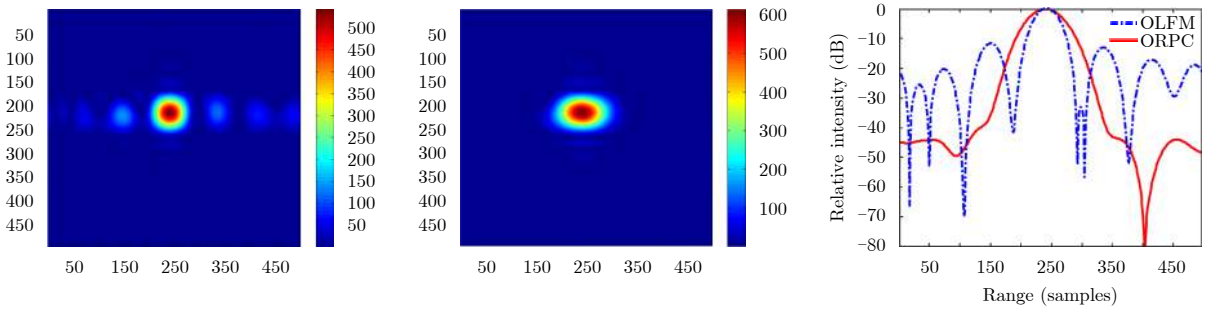

(a) Point target focused by using OLFM (b) Point target focused by using ORPC (c) Comparison of the range profiles

Fig. 8 Point target focused by using OLFM (a), and ORPC (b). Comparison of the range profiles were showed in (c).

of the proposed signals, the interfering signals will be suppressed by the matched filtering in the DSP of the sensor.

A representative experiment has been investigated on reducing of high interferences, in which the Signal to Interference Ratio (SIR) is 0 dB. Fig. 11

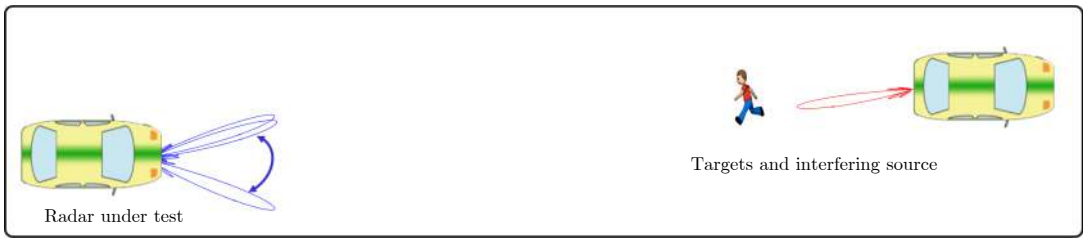

Fig. 9 A representative scenario designed for experiment

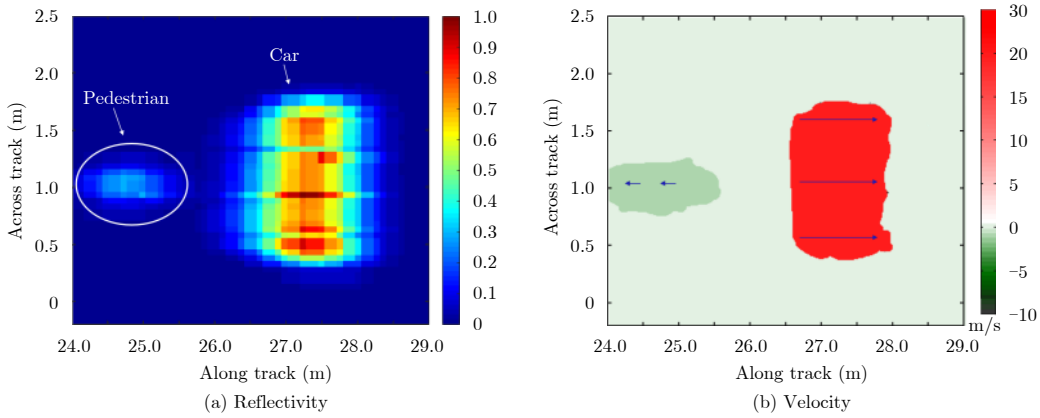

(a) Reflectivity (b) Velocity

Fig. 10 High-resolution imaging of range, azimuth and velocity for the targets.

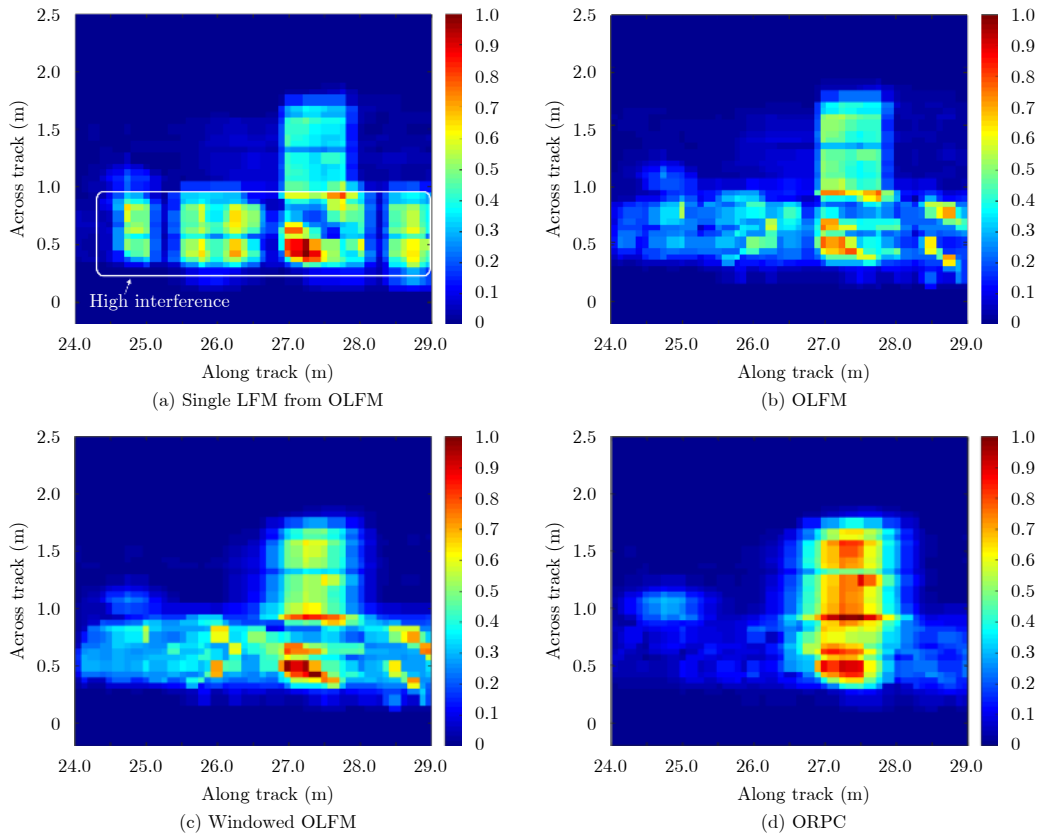

(a) Single LFM from OLFM (b) OLFM

(c) Windowed OLFM (d) ORPC

Fig. 11 Results on the presences of high interferences by using single LFM from OLFM (a), OLFM (b), Windowed OLFM (c), and ORPC (d), respectively.

demonstrates the results of the proposed sensor, using for types of transmitted signal, including single LFM, OLFM, windowed OLFM and the ORPC signals. The results suggest that a strategy of using a single FM signal cannot suppress the inter-sensor interfering signals. However, use of orthogonal signals can effectively reduce these undesired signals. By visual comparison, the image quality by the ORPC is better than that of OLFM and windowed OLFM. The SIR by using the OLFM, windowed OLFM and the ORPC is improved to 3.14 dB, 1.09 dB, and 14.47 dB, respectively.

4 Conclusion

In this paper, we have proposed a novel automotive radar for sensing the road environment in high resolution. The proposed DBF transmitter improves the spatial resolution in the azimuth for the sensor. The bistatic antenna architecture offers the close range detection for adapting to automotive applications. The proposed ORPC signals benefit the sensor high processing gain and high resolution in range. Furthermore, the ORPC signals provide lower sidelobe levels without any loss of SNR for the sensor. Interestingly, the interferences of the neighboring radar have been significantly reduced by using the ORPC signals. The representative simulation results have demonstrated the advantage of the proposed radar and might be promising features for automotive applications.

References

[1] Abou-Jaoude R. ACC radar sensor technology, test requirements, and test solutions[J]. *IEEE Transactions on Intelligent Transportation Systems*, 2003, 4(3): 115–122. DOI: 10.1109/TITS.2003.821286.

[2] Patole S M, Torlak M, Wang D, *et al.*. Automotive radars: A review of signal processing techniques[J]. *IEEE Signal Processing Magazine*, 2017, 34(2): 22–35. DOI: 10.1109/MSP.2016.2628914.

[3] Kronauge M and Rohling H. New chirp sequence radar waveform[J]. *IEEE Transactions on Aerospace and Electronic Systems*, 2014, 50(4): 2870–2877. DOI: 10.1109/TAES.2014.120813.

[4] Wu S G, Decker S, Chang P, *et al.*. Collision sensing by stereo vision and radar sensor fusion[J]. *IEEE Transactions on Intelligent Transportation Systems*, 2009, 10(4): 606–614. DOI: 10.1109/TITS.2009.2032769.

[5] Gresham I, Jain N, Budka T, *et al.*. A compact manufacturable 76–77 GHz radar module for commercial ACC applications[J]. *IEEE Transactions on Microwave Theory and Techniques*, 2001, 49(1): 44–58. DOI: 10.1109/22.899961.

[6] Tsang S H, Hall P S, Hoare E D, *et al.*. Advance path measurement for automotive radar applications[J]. *IEEE Transactions on Intelligent Transportation Systems*, 2006, 7(3): 273–281. DOI: 10.1109/TITS.2006.880614.

[7] Guo Kun-Yi, Hoare E G, Jasteh D, *et al.*. Road edge recognition using the stripe Hough transform from millimeter-wave radar images[J]. *IEEE Transactions on Intelligent Transportation Systems*, 2015, 16(2): 825–833. DOI: 10.1109/TITS.2014.2342875.

[8] Mao X S, Inoue D, Matsubara H, *et al.*. Demonstration of in-car doppler laser radar at 1.55 μm for range and speed measurement[J]. *IEEE Transactions on Intelligent Transportation Systems*, 2013, 14(2): 599–607. DOI: 10.1109/TITS.2012.2230325.

[9] Lee J E, Lim H S, Jeong S H, *et al.*. Enhanced iron-tunnel recognition for automotive radars[J]. *IEEE Transactions on Vehicular Technology*, 2016, 65(6): 4412–4418. DOI: 10.1109/TVT.2015.2460992.

[10] Kellner D, Barjenbruch M, Klappstein J, *et al.*. Tracking of extended objects with high-resolution doppler radar[J]. *IEEE Transactions on Intelligent Transportation Systems*, 2016, 17(5): 1341–1353. DOI: 10.1109/TITS.2015.2501759.

[11] Wang X, Xu L H, Sun H B, *et al.*. On-road vehicle detection and tracking using MMW radar and monovision fusion[J]. *IEEE Transactions on Intelligent Transportation Systems*, 2016, 17(7): 2075–2084. DOI: 10.1109/TITS.2016.2533542.

[12] Wang H N, Huang Y W, and Chung S J. Spatial diversity 24-GHz FMCW radar with ground effect compensation for automotive application[J]. *IEEE Transactions on Vehicular Technology*, 2017, 66(2): 965–973. DOI: 10.1109/TVT.2016.2565608.

[13] Askeland S A and Ekman T. Tracking with a high-resolution 2D spectral estimation based automotive radar[J]. *IEEE Transactions on Intelligent Transportation Systems*, 2015, 16(5): 2418–2423. DOI: 10.1109/TITS.2015.2407571.

[14] Lee M S and Kim Y H. Design and performance of a 24-GHz switch-antenna array FMCW radar system for automotive applications[J]. *IEEE Transactions on Vehicular Technology*, 2010, 59(5): 2290–2297. DOI: 10.1109/TVT.2010.2045665.

[15] Hu C X, Liu Y M, Meng H D, *et al.*. Randomized switched antenna array FMCW radar for automotive applications[J]. *IEEE Transactions on Vehicular Technology*, 2014, 63(8):

3624–3641. DOI: 10.1109/TVT.2014.2308895.

[16] Shirakawa K. PRISM: An in-vehicle CPU-oriented novel azimuth estimation technique for electronic-scan 76-GHz adaptive-cruise-control radar system[J]. *IEEE Transactions on Intelligent Transportation Systems*, 2008, 9(3): 451–462. DOI: 10.1109/TITS.2008.922979.

[17] Dudek M, Nasr I, Bozsik G, *et al.*. System analysis of a phased-array radar applying adaptive beam-control for future automotive safety applications[J]. *IEEE Transactions on Vehicular Technology*, 2015, 64(1): 34–47. DOI: 10.1109/TVT.2014.2321175.

[18] Gambi E, Chiaraluce F, and Spinsante S. Chaos-based radars for automotive applications: Theoretical issues and numerical simulation[J]. *IEEE Transactions on Vehicular Technology*, 2008, 57(6): 3858–3863. DOI: 10.1109/TVT.2008.921632.

[19] Cheng P, Zhang F, Chen J M, *et al.*. A distributed TDMA scheduling algorithm for target tracking in ultrasonic sensor networks[J]. *IEEE Transactions on Industrial Electronics*, 2013, 60(9): 3836–3845. DOI: 10.1109/TIE.2012.2208439.

[20] Imana E Y, Yang T, and Reed J H. Addressing a neighboring-channel interference from high-powered radar[J]. *IEEE Transactions on Vehicular Technology*, 2016, 65(5): 2872–2882. DOI: 10.1109/TVT.2015.2442217.

[21] Richards M A. Fundamentals of Radar Signal Processing[M]. New York: McGraw-Hill, 2005.

[22] Shechtman Y, Eldar Y C, Cohen O, *et al.*. Phase retrieval with application to optical imaging: A contemporary overview[J]. *IEEE Signal Processing Magazine*, 2015, 32(3): 87–109. DOI: 10.1109/MSP.2014.2352673.

Xu Zhihuo received the Ph.D. degree in communication and information system in 2016, from the University of Chinese Academy of Sciences (UCAS) and the Institute of Electronics of the Chinese Academy of Sciences (IECAS), Beijing, China. He joined Radar and Image Research Group, School of transportation in Nantong University, China, in 2016, where he is currently a lecturer. His current research interests include advanced radar signal and image processing methodologies.
E-mail: xuzhihuo@gmail.com

Shi Quan was born in Haimen, China, in 1973. He is currently a professor in the School of Transpiration, Nantong University, China. He has authored more than 60 papers since 2007, of which more than 40 are peer-reviewed and well-known journal papers. His research is focused on the development of signal and image processing and big data techniques.
E-mail: sq@ntu.edu.cn

Sun Ling received the Ph.D. degree in circuit and system in 2008, from the Southeast University. She is currently a professor in the Jiangsu Key Laboratory of ASCI Design, Nantong University, China. Her research is focused on radio frequency circuit design and signal processing.
E-mail: sunl@ntu.edu.cn